IEEE Photonics Journal
An IEEE Photonics Society Publication

Open Access

Pre-Filtering Techniques for Spectrum Narrowing Caused by Optical Node Traversal in Ultra-Dense WDM Networks

Volume 13, Number 2, April 2021

Kazuya Okamura
Yojiro Mori, ***Member, IEEE***
Hiroshi Hasegawa, ***Member, IEEE***

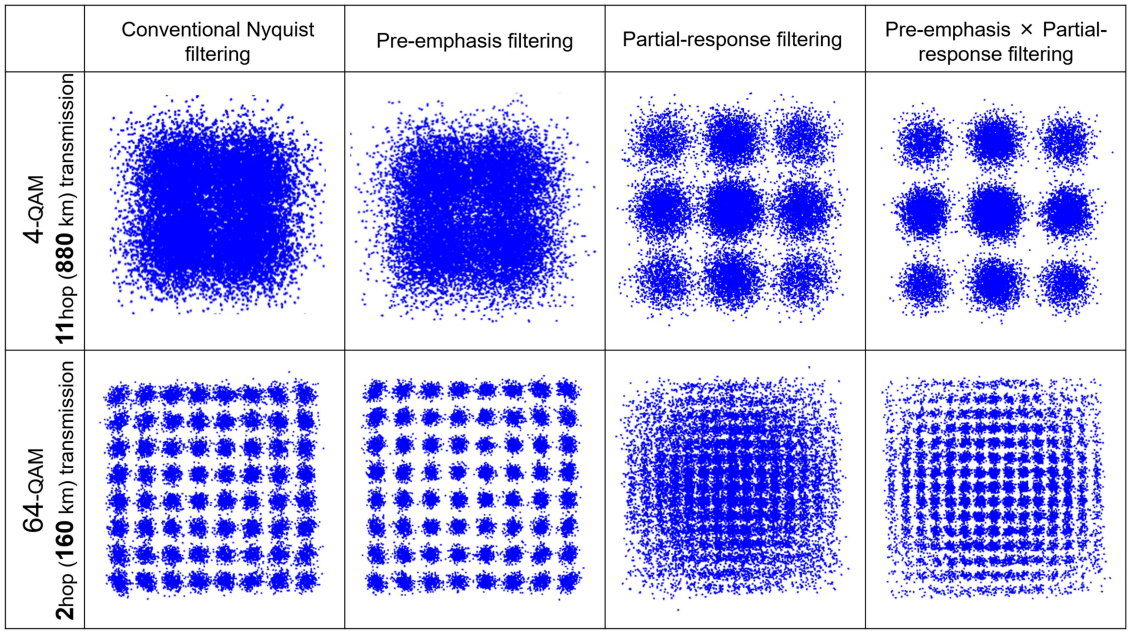

DOI: 10.1109/JPHOT.2021.3065139

IEEE photonics SOCIETY
IEEE

Pre-Filtering Techniques for Spectrum Narrowing Caused by Optical Node Traversal in Ultra-Dense WDM Networks

Kazuya Okamura, Yojiro Mori, *Member, IEEE*, and Hiroshi Hasegawa, *Member, IEEE*

Department of Information and Communication Engineering, Nagoya University, Nagoya 464-8603, Japan

DOI:10.1109/JPHOT.2021.3065139

Manuscript received December 24, 2020; revised February 23, 2021; accepted March 7, 2021. Date of publication March 11, 2021; date of current version March 31, 2021. This work was supported in part by NICT, in part by the MIC/SCOPE (192106002), and in part by the KAKENHI (18K13756). Corresponding author: Kazuya Okamura (e-mail: k_okamur@nuee.nagoya-u.ac.jp).

Abstract: To improve the spectral efficiency and increase network capacity, wavelength signals must be multiplexed densely, i.e., ultra-dense wavelength-division-multiplexing (WDM) networks. However, the spectrum of each WDM signal is narrowed by the wavelength-selective switches placed in optical nodes, so the transmissible distance and node hop count of the signal are strictly limited. To counter this spectrum narrowing problem caused by optical node traversal in ultra-dense WDM networks, pre-filtering techniques have been proposed. This paper comprehensively investigates the performance of four pre-filtering techniques: conventional Nyquist filtering, pre-emphasis filtering, partial-response filtering, and the combination of pre-emphasis and partial-response filtering. We conduct extensive computer simulations and discuss the optimality of pre-filtering techniques. The simulation results show that the adaptive use of pre-filtering can substantially extend the maximum attainable transmission distance and hop counts of 4/16/64-QAM signals.

Index Terms: Photonic network, optical node, higher-order modulation, digital coherent system.

1. Introduction

In photonic networks, optical nodes based on wavelength-selective switches (WSSs) can transparently route wavelength-division-multiplexing (WDM) signals without costly optical-to-electrical and electrical-to-optical conversion. To fulfil the demand for greater network capacity while retaining cost-effectiveness, we need to adopt ultra-dense WDM systems in which the bandwidth of guardbands placed between neighboring WDM signals is smaller than that of present dense WDM systems [1]. In such systems, however, the impact of the spectrum-narrowing impairment caused by traversing WSSs in optical nodes is significant [2]–[11]. Spectrum narrowing induces intersymbol interference (ISI) because the overall transfer function of WSSs does not meet the Nyquist criterion. Furthermore, the optical amplifiers used to offset the fiber loss add amplified-spontaneous-emission (ASE) noise to the signals filtered by WSSs. Through these filtering-and-amplification processes, the ISI and the ASE noise impair the signal in an interactive manner. The ISI itself can be compensated by linear post-compensation filters in digital coherent receivers [12],

[13]. However, ISI compensation at the receiver side degrades overall signal-to-noise ratio (SNR) since the lower-power frequency components created by WSS filtering are magnified [14].

The SNR degradation due to ISI compensation can be alleviated by pre-emphasis filtering [15]–[17]. In this scheme, frequency components that will be attenuated by node traversal are partly emphasized using transmitter-side digital signal processing (DSP) so that noise enhancement by post-compensation filtering is suppressed. However, excess power loss is induced at each node traversal since pre-emphasis allocates larger power to more lossy frequency components. Consequently, excess SNR degradation increases with the node-hop count. Another possible solution, partial-response coding, alleviates noise enhancement at the receiver side. The partial-response filter reduces the 3 dB bandwidth of the signal spectrum by allowing deterministic ISI [18]–[21]. Then, maximum likelihood sequence estimation (MLSE) conducts symbol decision under the residual deterministic ISI [18]; nevertheless, noise enhancement is still inevitable since the partial-response filter does not reduce the overall signal bandwidth. In addition, the shortened inter-symbol distances on the constellation map result in lower tolerance against ASE noise and fiber nonlinearity. The combination of pre-emphasis filtering and partial-response filtering is also possible [22]. This scheme simultaneously utilizes a pre-emphasis filter that emphasizes the spectral edges and a partial-response filter that suppresses the spectral edges within the transmitter-side DSP circuit. The two filters, which have different features, can achieve low excess power loss at each node and suppressed noise enhancement in the receiver. However, the short inter-symbol distances due to partial-response filtering would degrade the noise tolerance. Thus, the effectiveness of each scheme varies according to system conditions such as filtering characteristics and noise characteristics. In order to use pre-filtering techniques efficiently, we need to clarify the application extent of each pre-filtering technique while changing the system conditions.

In this paper, we investigate the transmission characteristics of four pre-filtering schemes and clarify their appropriateness. Although such a filtering process can be done in both digital and optical domains [23], we discuss here the digital approach. Performance is analyzed using a wide range of parameters including modulation order, node structure, repeater-span length, link length, and network scale. Extensive computer simulations show that the appropriate pre-filtering scheme can extend the maximum transmissible lengths and hop counts of 4/16/64-QAM signals in ultra-dense WDM networks. The remainder of this paper is organized as follows: Section 2 details pre-filtering techniques that can alleviate the spectrum narrowing impairment. Section 3 evaluates the performance of four pre-filtering schemes through extensive computer simulations. Finally, this paper is concluded in Section 4.

2. Pre-filtering Schemes

2.1 Pre-emphasis Filtering

A pre-emphasis filter enhances the spectral edges of the signal in advance so as to counteract the wavelength-dependent power attenuation due to WSS traversal. Insufficient emphasis cannot attain complete compensation of spectrum narrowing while excessive emphasis results in excessive power loss at each WSS traversal. Therefore, filter optimization for each system is required. Let us derive the pre-emphasis filter that offers the highest SNR under the ISI-free condition [15]. Fig. 1 illustrates a typical transmission model of optical networks, where the broadcast-and-select node architecture is assumed for simplicity [24]. In the transmitter DSP circuit, the desired signal, $S_t(f)$, is shaped by the pre-filter $C_t(f)$. In the source node, the signal is added to a network by a WSS $W_0(f)$. After amplification using an erbium-doped fiber amplifier (EDFA), the signal enters a transmission link. In the link, the signal experiences attenuation and amplification, and the signal spectrum is contaminated by ASE noise. Typically, ASE noise can be regarded as white Gaussian noise within the channel bandwidth. After traversing the link, the signal enters the next node. In the *m*-th node, the signal is filtered by a WSS, $W_m(f)$, for wavelength routing. After h node hops, the signal is dropped using a splitter and digital coherent receiver. Here, let the transfer function of cascaded WSSs be $W_{total}(f)$ and the accumulated ASE noise be N(f). Note that the ASE noise is also filtered

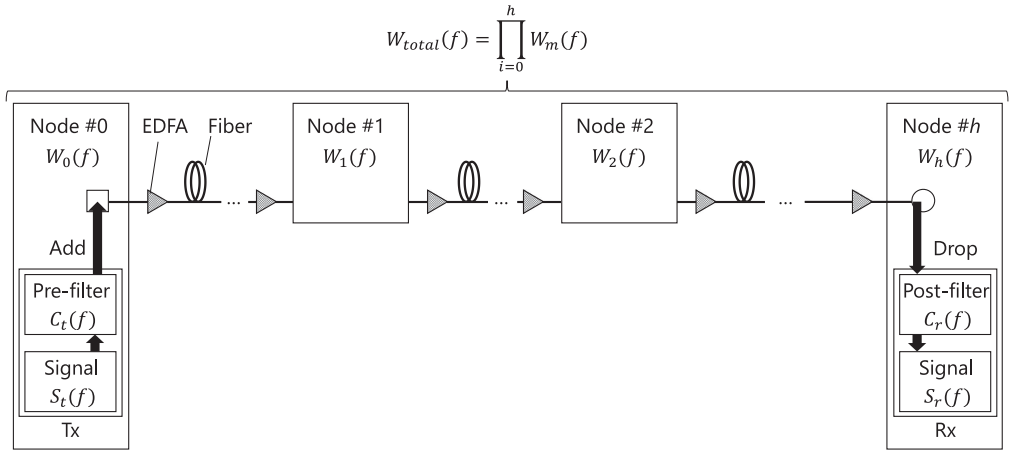

Fig. 1. Transmission model for deriving the optimum pre-emphasis filter.

at each WSS traversal and hence N(f) is no longer white Gaussian noise. After post-compensation filtering $C_r(f)$ in the digital coherent receiver, we obtain the recovered signal, $S_r(f)$. Here, $S_r(f)$ is given as

$$S_r(f) = S_t(f)\, C_t(f)\, W_{\text{total}}(f)\, C_r(f) + N(f)\, C_r(f) \tag{1}$$

where the first and second terms denote the signal and the noise, respectively. Since the ISI-free condition is given by $C_t(f)W_{total}(f)C_r(f) = 1$, (1) can be rewritten as

$$S_r(f) = S_t(f) + N(f)\, C_t(f)^{-1} W_{\text{total}}(f)^{-1} \tag{2}$$

Under the ISI-free condition, maximization of the SNR, i.e., minimization of noise power while retaining signal power, is given by

$$\begin{aligned} &\text{minimize} \int_{-\infty}^{\infty} \left| N(f)\, C_t(f)^{-1} W_{\text{total}}(f)^{-1} \right|^2 df \\ &\text{subject to} \int_{-\infty}^{\infty} C_t(f)\, df = 1 \end{aligned} \tag{3}$$

We can solve this variational problem as shown in appendix and pre-filter $C_t(f)$ is given as

$$C_t(f) = \mu_t \left| \frac{N(f)}{W_{\text{total}}(f)} \right|^{\frac{2}{3}} \tag{4}$$

where μ_t is denoted as a power normalization factor. It is noteworthy that the ISI-free condition is not always the best solution. Therefore, let us define the pre-emphasis filter using pre-emphasis strength k as

$$C_t(f) = \mu_t \left| \frac{N(f)}{W_{\text{total}}(f)} \right|^{k} \tag{5}$$

Note that N(f) can be obtained by using a receiver or performance monitor. When no signal or continuous wave is transmitted, we can directly observe the received noise spectrum, N(f). The information obtained by the receiver or performance monitor is transferred over the optical supervisory channel.

Another critical issue with pre-emphasis filters is excess power loss due to node traversal. For example, let us assume that we allocate the signal power of 10 mW between two frequencies, f_1 and f_2, where f_1 yields loss of 3 dB while f_2 yields loss of 6 dB. If we allocate 5 mW to f_1 and 5 mW

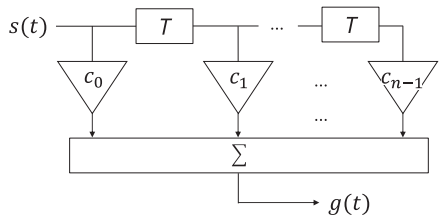

Fig. 2. Partial-response filter.

to f_2 (*i.e.*, the conventional scheme), the overall output power becomes ~3.76 mW. If we allocate higher power to the more lossy frequency like 2 mW to f_1 and 8 mW to f_2 (*i.e.*, pre-emphasis scheme), the overall output power becomes ~3.01 mW, which is less than the former scheme. In this way, the overall insertion loss of a WSS depends on the power distribution of the optical signal. Since the overall loss increases at each node, the SNR at the receiver is severely decreased when the hop count is large. To avoid this problem, the pre-emphasis filters need to be used in conjunction with inline channel-by-channel power compensation: First, all the WDM signals in a fiber are over-amplified with an EDFA. Then, the following WSS within the node sets the power to the prescribed level in a channel-by-channel manner. Note that inline power control is widely adopted in present networks so as to flatten WDM signal powers. We can thus compensate for the excess filtering loss without additional hardware.

2.2 Partial-response Filtering

A partial response filter enables narrow 3 dB signal bandwidth in return for some level of ISI. Fig. 2 is a schematic of the partial-response filter, where s(t) is the input signal, T the symbol duration, *i* the tap number, *n* the number of taps, c_i the *i*-th tap coefficient, and g(t) is the output signal. Here, *g*(t) is written as

$$g(t) = \sum_{i=0}^{n-1} c_i s(t - iT) \tag{6}$$

Applying the Fourier transform, we obtain the transfer function of the partial-response filter H(f) as

$$H(f) = \sum_{i=0}^{n-1} c_i \cdot \exp(-j2\pi f_i T) \tag{7}$$

If, as an example, the duo-binary filter is applied, the transfer function can be derived by setting $n = 2$ and $c_0 = c_1 = 1$ in (7);

$$H(f) = \begin{cases} 2T\cos\pi fT & |f| \le \frac{1}{2T} \\ 0 & \text{otherwise} \end{cases} \tag{8}$$

If f_c is the 3 dB cut-off frequency, we can write

$$2T\cos\pi f_c T = \frac{1}{\sqrt{2}} \cdot 2T \tag{9}$$

$$\pi f_c T = \pm\frac{\pi}{4} \tag{10}$$

$$f_c = \pm\frac{1}{4T} \tag{11}$$

This result means that the duo-binary filter can halve the 3 dB bandwidth of the signal spectrum. In this way, the partial-response filter achieves narrow 3 dB bandwidth. In other words, the partial-response filter allocates signal power to frequencies close to the carrier frequency and avoid

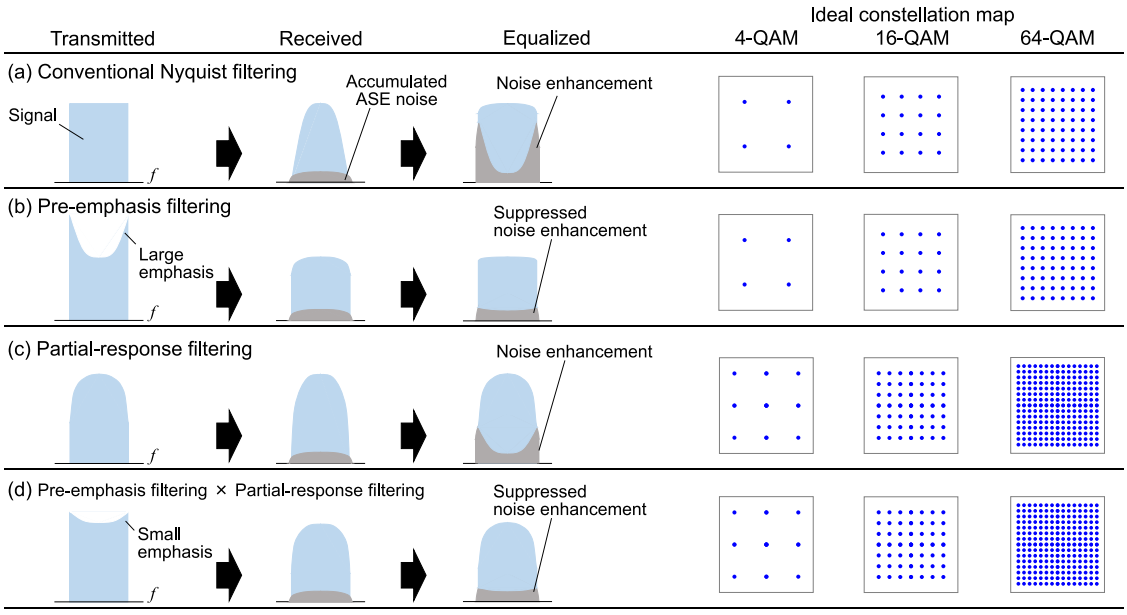

Fig. 3. Four candidates for spectrum shaping.

lossy frequencies. Therefore, partial-response filtering can obtain high tolerance against spectrum narrowing. However, the controlled ISI shortens the inter-symbol distances on the constellation map; consequently, the signal after partial-response filtering is more susceptible to ASE noise and fiber nonlinearity.

2.3 Comparison of Pre-Filtering Schemes

Fig. 3 compares four transmitter-side pre-filtering schemes: (a) conventional Nyquist filtering, (b) pre-emphasis filtering, (c) partial-response filtering, and (d) a combination of pre-emphasis filtering and partial-response filtering. In most present coherent transmission systems, the signal spectrum is formed by a Nyquist filter. The signal repeatedly experiences filtering by WSSs and contamination by ASE noise along the transmission line. Linear post-compensation filters in the digital coherent receiver can compensate for the ISI caused by spectrum narrowing. Adaptive filters used to compensate for polarization-mode dispersion try to undo ISI as well. This filtering process magnifies the power of low-SNR frequency components and so exacerbates the overall SNR [14]. The pre-emphasis filter converges the signal power on lossy frequency components by using the transmitter-side DSP circuit [15]–[17]. This process counteracts the spectrum narrowing induced by WSS traversal. Consequently, the noise enhancement induced by post-compensation filtering is alleviated. However, each WSS traversal causes excess power loss and thus pre-emphasis filtering must set larger power levels to attain larger node-hop counts. Owing to the limitation of the fiber input power, the effectiveness of pre-emphasis filtering declines with higher hop counts. As for partial-response filtering, the impact of spectrum narrowing is small thanks to its originally narrow signal bandwidth [19]–[21]. However, the number of symbol states is increased due to deterministic ISI. If two-symbol-length ISI is considered, the numbers of symbol states of 4-QAM, 16-QAM, 64-QAM signals are 9, 49, and 225, respectively. The short inter-symbol distances on the constellation map degrades noise tolerance. Moreover, the post-compensation filter preceding MLSE inevitably enhances the noise as in conventional Nyquist-filtering systems. The combination filter combines pre-emphasis filtering and partial-response filtering. The former suppresses the noise enhancement caused by post-compensation filtering. In addition, the partial-response filtering

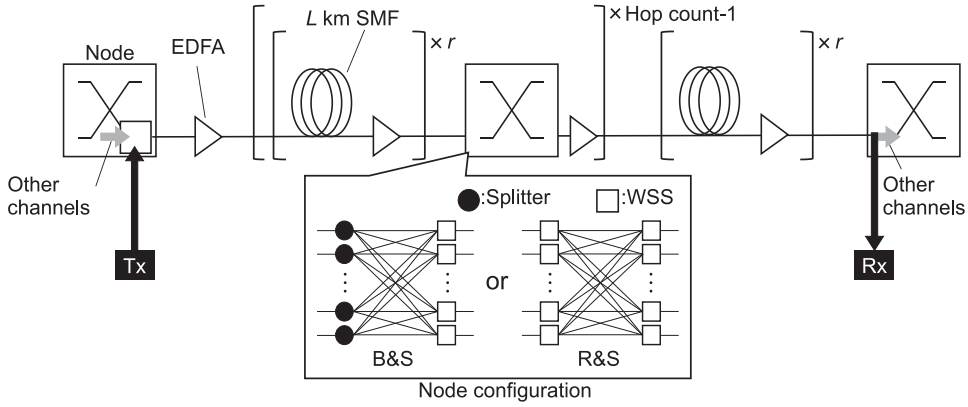

Fig. 4. Simulation setup.

suppresses the excess node loss caused by pre-emphasis filtering by reducing the emphasis power needed [21]. However, lower noise tolerance due to partial-response filtering is still a problem.

3. Simulations

To assess the applicable areas of these pre-filtering schemes, we conducted extensive computer simulations. Our simulations consider the impact of fiber nonlinearity and the oversampling ratio is set to 11. Fig. 4 illustrates the simulation setup. A transmitter generates a 32-Gbaud dual-polarization (DP) 4/16/64-QAM signal. The spectrum is basically formed by a Nyquist filter with a roll-off factor of 10^{-2}. In addition, a pre-emphasis filter, partial-response filter, or combination of a pre-emphasis filter and partial-response filter is applied. The pre-emphasis filter, $C_t(f)$, is given by (5). The pre-emphasis strength, k, is optimized for each system at the resolution of 1/6, so that the bit error ratio (BER) is minimized. We assumed the use of ideal digital-to-analog and analog-to-digital converters. The transmitter laser has a linewidth of 100 kHz. The signal is added to the network through a WSS and multiplexed with eight non-target signals that are closest to the target signal in the frequency domain. The frequency interval of the WDM signals is 37.5 GHz. We created the WSS filter by convoluting a rectangular function with 37.5 GHz bandwidth and a Gaussian function with 10-GHz 3-dB bandwidth [25]. The resulting 6 dB bandwidth is 37.5 GHz. The port isolation of the WSS is 30 dB. After an EDFA, the signals enter a repeater span of a 40-km or 80-km single-mode fiber (SMF). The signal power launched into the SMF is optimized in each system at the resolution of 1dB. The optimized launch power lies in the range of -3 to -7 dBm per channel. The noise figure of the EDFA is 5 dB. The starting OSNR within the signal bandwidth ranges 39 to 43 dB depending on the launch power. The loss coefficient, chromatic-dispersion parameter, and nonlinear coefficient of the SMF are 0.2 dB/km, 17 ps/nm/km, and 1.5 /W/km, respectively. The interaction among loss, chromatic dispersion, and fiber nonlinearity is calculated by the conventional split-step Fourier method [26]. The 8×8 optical nodes are configured in the broadcast-and-select (B&S) or route-and-select (R&S) manner [24]. The node insertion loss is basically 16.5 dB for the B&S configuration and 14 dB for the R&S configuration. Although the number of spectrum-narrowing events can be reduced by using the impairment-aware routing and wavelength-assignment algorithm [5], we assume the worst case where the signal spectrum is narrowed at every node traversal; the number of filtering operations at every node is 1 for the B&S architecture and 2 for the R&S architecture. After multiple node hops, the target signal is dropped through a splitter in B&S nodes or through a WSS in R&S nodes. The target signal is then detected by a digital coherent receiver. The local oscillator has a 100 kHz linewidth. After down-sampling to 64 Gsample/s, the signal is delivered to a DSP circuit. In the receiver DSP circuit, chromatic dispersion is undone by a fixed filter. The post compensation filter with 64 taps adapted by the

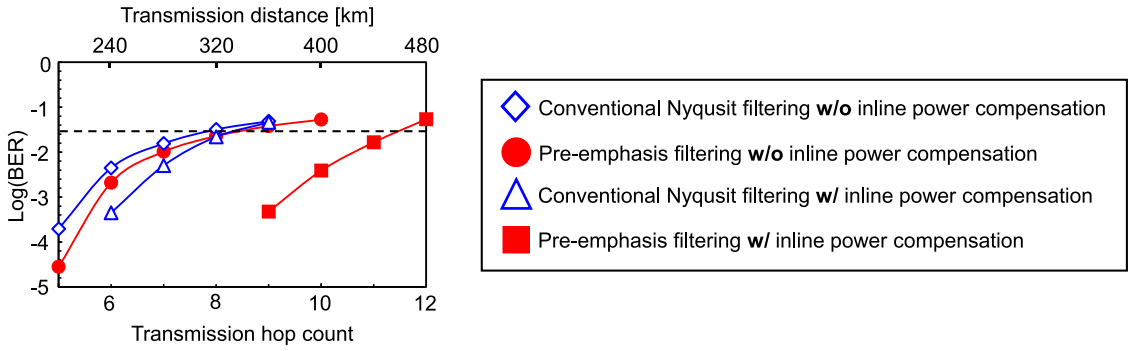

Fig. 5. BER versus hop count; necessity of inline power compensation for utilizing pre-emphasis filtering.

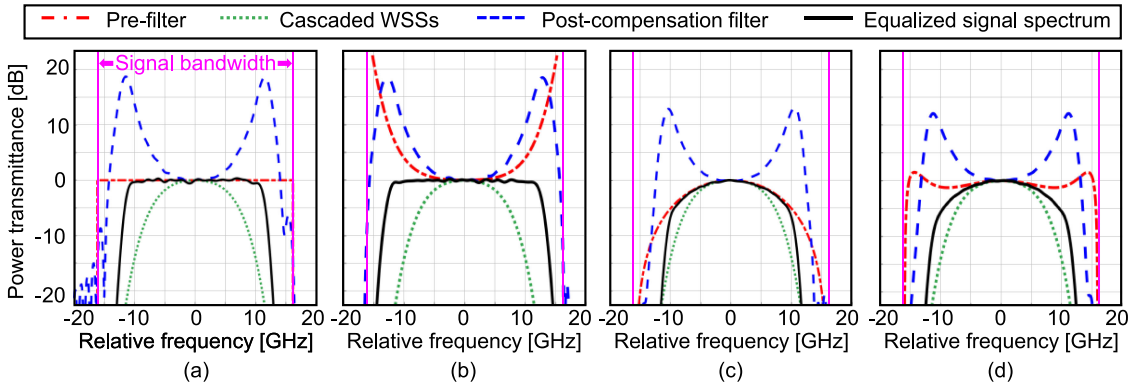

Fig. 6. Examples of transfer functions and equalized signal spectra, where the pre-filter is changed.

least-mean-square (LMS) algorithm then executes polarization demultiplexing and signal-spectrum reshaping [12], [13]; the length of training symbols was 81920. After that, the carrier phase and frequency are estimated. Finally, the signal is decoded; when the partial-response filter is adopted, the conventional MLSE decodes the signals under the residual two-symbol-length ISI [18]. The target BER is 2.7×10^{-2} presupposing the use of forward-error correction (FEC) with a 20% overhead [27].

First, we confirm the performance of pre-emphasis filters. Fig. 5 plots BER versus hop count of 4-QAM signals; we tested pre-emphasis filtering with and without inline power compensation. Here, we assume the use of the R&S node architecture. The inter-node distance is set to 40 km. We observe that pre-emphasis filtering without inline compensation only slightly increases attainable hop count, while pre-emphasis with inline power compensation significantly enhances performance. Thus, the pre-emphasis must be utilized in conjunction with inline power compensation; hereinafter pre-emphasis filtering is applied jointly with inline power compensation.

Fig. 6 depicts examples of transfer functions of the pre-filter, cascaded WSSs, and post-compensation filter and equalized signal spectra. The pre-filter shown in Fig. 6(a) is just the conventional Nyquist filter; The pre-filters shown in Fig. 6(b), Fig. 6(c), and Fig. 6(d) are a pre-emphasis filter, a partial-response filter, and a combination of a pre-emphasis filter and a partial-response filter, respectively. Here, a 4-QAM signal after 11 node-hop transmission is shown as an example. We assumed the use of the R&S node configuration. The inter-node distance is 80 km, and each link consists of an 80 km SMF and an EDFA. The peak to average power ratios measured at the transmitter side are 7.2 dB, 9.2 dB, 4.6 dB, and 8.2 dB for the respective cases. In Fig. 6(a), we

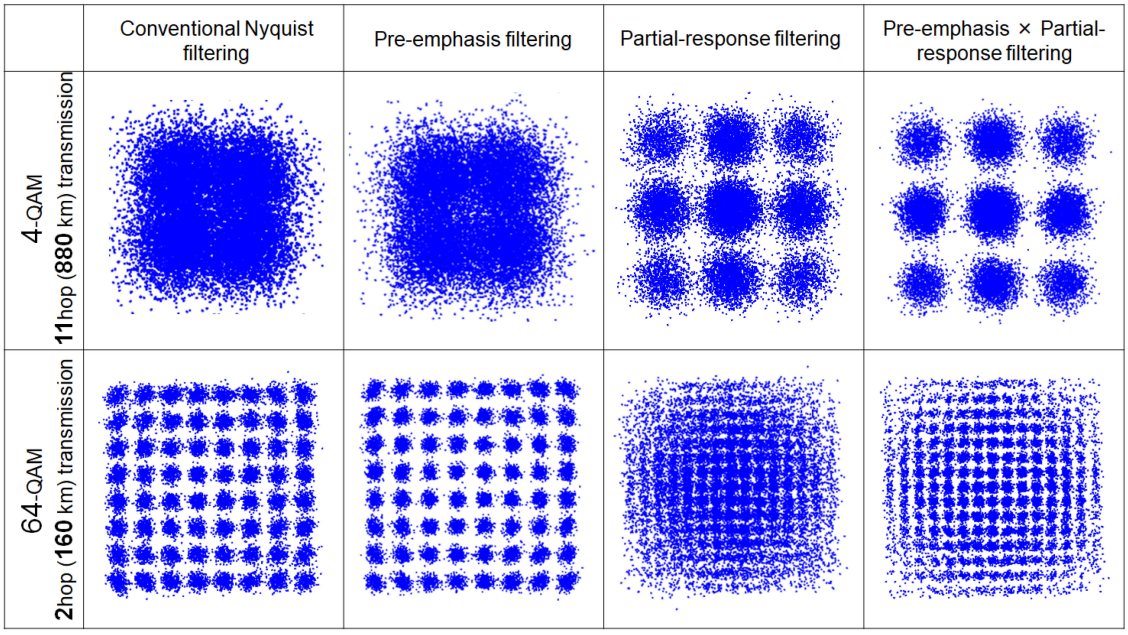

Fig. 7. Constellation maps after post-filtering.

observe that the bandwidth of the equalized signal spectrum is much smaller than the original signal bandwidth. This is because the post-compensation filter alone does not sufficiently eliminate ISI so as to avoid noise enhancement. Consequently, the residual ISI degrades the signal quality. As for Fig. 6(b), the bandwidth of the equalized signal spectrum is expanded by the pre-emphasis filter while the noise-enhancement level is retained; in other words, the pre-emphasis filter can maintain the noise-enhancement level while eliminating more ISI. However, the noise enhancement due to the post-compensation filter is still significant. In Fig. 6(c), the noise enhancement is small thanks to the narrow bandwidth. The scheme shown in Fig. 6(d) offers smaller emphasis than the scheme in Fig. 6(b) and larger bandwidth than that in Fig. 6(c). In other words, this scheme yields, simultaneously, small excess loss at each node and small noise enhancement at the receiver.

Constellation maps after post-compensation filtering are shown in Fig. 7. The use of R&S nodes is assumed. The transmission hop count is 11 for a 4-QAM signal and 4 for a 64-QAM signal. In 4-QAM systems, partial-response filtering increases the number of symbol states from 4 to 9 due to deterministic two-symbol-length ISI. In this case, the combination of pre-emphasis filtering and partial-response filtering scheme attains the highest SNR. On the contrary, partial-response filtering hinders the symbol decision of 64-QAM signals because inter-symbol distance is severely shortened due to deterministic ISI; the number of symbol states increases from 64 to 225. Thus, the optimum pre-filter depends on system parameters.

Fig. 8 plots BER versus transmission hop count assuming transmission in metro networks; 4/16/64-QAM signals are transmitted in B&S-node systems or R&S-node systems whose inter-node distances are 40 km or 80 km. The pre-emphasis strength, k, is optimized for each system. We find that the combination of pre-emphasis and partial-response filtering is effective when spectrum-narrowing impairment is prominent. As for 4-QAM-signal transmission, the combination of pre-emphasis filtering and partial-response filtering substantially extends the maximum hop counts; the increments are up to 15 for 40 km systems and 13 for 80 km systems. In contrast, partial-response filtering negatively impacts 64-QAM-signal transmission. In these cases, the pre-emphasis scheme is useful; the hop-count extensions are up to 2 for 40 km systems and 2 for 80 km systems. As for 16-QAM-signal transmission, the best pre-filter changes with the node architecture and link length. This variation depends on which impairment is dominant; ASE noise is

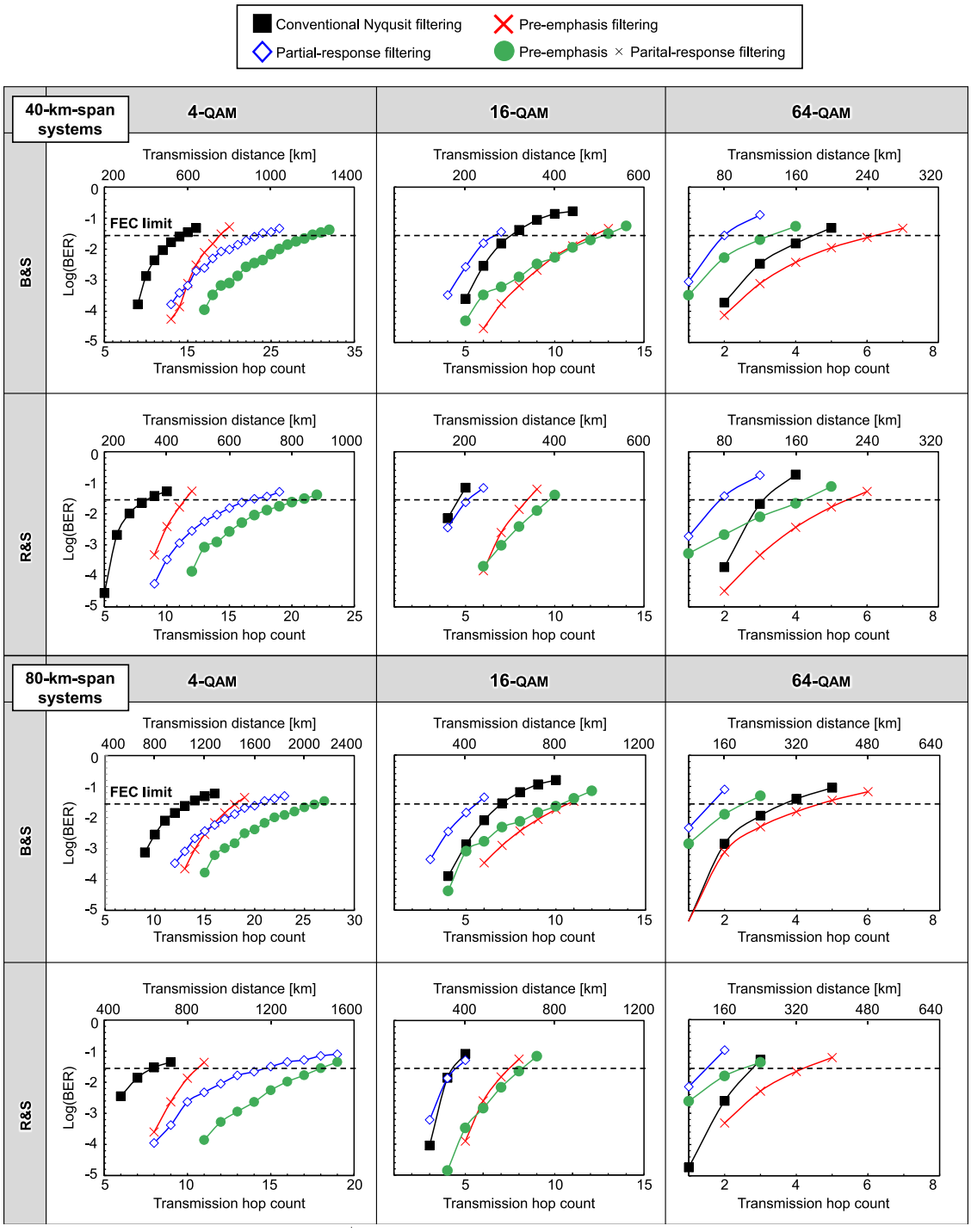

Fig. 8. BER versus transmission hop count in metro networks.

dominant in 80-km-span B&S node systems, whereas spectrum narrowing is more significant than ASE noise in the other systems. Thus, we need to select the appropriate pre-filtering scheme for each metro network.

We also executed transmission simulations assuming backbone networks. Fig. 9 plots BER versus transmission hop count of 4-QAM signals for B&S-node systems and R&S-node systems. The

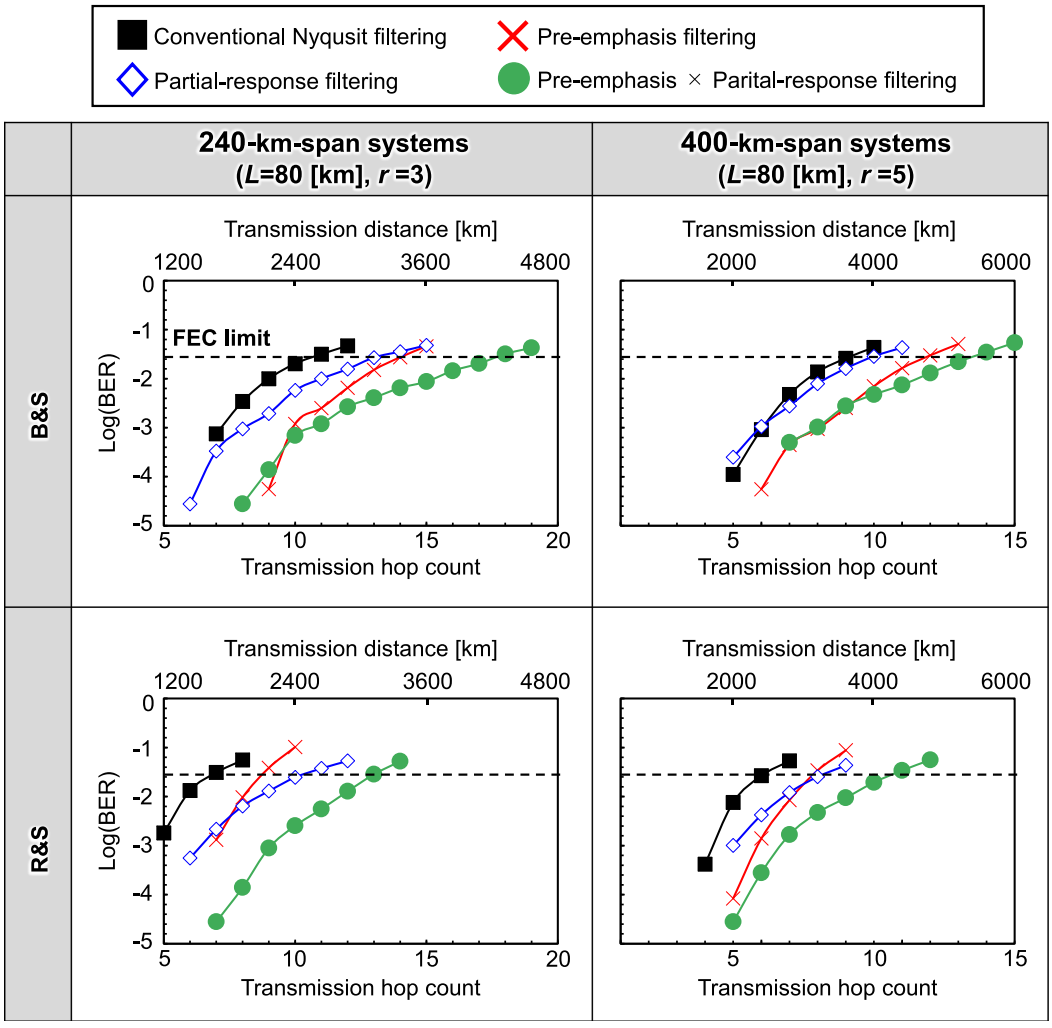

Fig. 9. BER versus transmission hop count in backbone networks, where r indicates the number of repeater spans of each link, see Fig. 4.

inter-node distances are 240 km and 400 km, while the repeater span is 80 km in both cases. The pre-emphasis strength, k, is optimized for each system. We observe that partial-response-filtered 4-QAM signals can achieve better performance in long-haul transmission as in metro networks in spite of its lower noise tolerance. We find that the use of the combination of pre-emphasis and partial-response coding can prominently extend the maximum transmission distance; the increase in transmission distances are up to 1680 km for 240-km-link systems and 2000 km for 400-km-link systems. Thus, the combination of pre-emphasis and partial-response filtering scheme is effective for distance extension in backbone networks.

4. Conclusion

We evaluated pre-filtering techniques to counter the spectrum narrowing impairment caused by optical node traversal in ultra-dense WDM networks. Extensive computer simulations showed that adopting the suitable pre-filtering scheme could drastically increase the attainable node-hop count compared to the conventional Nyquist filtering scheme in both metro-scale networks and backbone-scale networks. Simulations considered 32 Gbaud signals that are basically shaped with a Nyquist

filter with a roll-off factor of 10^{-2}, where the 6 dB bandwidth of each WSS was set to 37.5 GHz. As for metro networks, the increments in maximum hop count are up to 15 for 4-QAM, 6 for 16-QAM, and 2 for 64-QAM signal. Moreover, the increments of the transmission hop count of 4-QAM signals in backbone networks is up to 7 for 240-km-span systems and 5 for 400-km-span systems; corresponding distance extensions are 1680 km and 2000 km. The conventional Nyquist filtering scheme is not optimal for any of the tested conditions; in other words, appropriate use of pre-filtering techniques can expand the capacity of photonic networks. It is noteworthy that another scheme is the use of a whitening matched filter that can flatten the noise spectrum by accepting residual ISI; the resulting ISI is then mitigated by MLSE. When the impulse response of the channel is long due to severe spectrum narrowing, long-length MLSE is necessary. Thus, the whitening matched filter may further enhance the transmission performance with the penalty being an increase in calculation cost [28].

Appendix

In this appendix, we derive the pre-emphasis filter that maximizes SNR under the ISI-free condition. The variational problem shown in (3) is written as follows:

$$\begin{aligned} &\text{minimize} \int_{-\infty}^{\infty} \left| N(f)\, C_t(f)^{-1} W_{\text{total}}(f)^{-1} \right|^2 df \\ &\text{subject to} \int_{-\infty}^{\infty} C_t(f)\, df = 1 \end{aligned} \tag{A-1}$$

Applying the method of Lagrange multipliers, we obtain the functional as

$$I(C_t(f)) = \int_{-\infty}^{\infty} \left| \frac{N(f)}{C_t(f)\, W_{\text{total}}(f)} \right|^2 df + \mu \left\{ \int_{-\infty}^{\infty} C_t(f)\, df - 1 \right\} \tag{A-2}$$

where μ is an arbitrary finite number. We substitute $C_t(f) + \varepsilon\delta(f)$ for $C_t(f)$;

$$I(C_t(f) + \varepsilon\delta(f)) = \int_{-\infty}^{\infty} \left| \frac{N(f)}{\{C_t(f) + \varepsilon\delta(f)\}\, W_{\text{total}}(f)} \right|^2 df + \mu \left\{ \int_{-\infty}^{\infty} \{C_t(f) + \varepsilon\delta(f)\}\, df - 1 \right\} \tag{A-3}$$

where ε is a complex number and $\delta(f)$ is a minute complex vector. The partial derivative of (A-3) by ε corresponds to the partial directional derivative of $I(C_t(f))$ by $\delta(f)$. Since functional $I(C_t(f))$ is a convex function, $I(C_t(f))$ is minimized when the directional derivative is zero. The partial derivative of (A-3) by ε is written as

$$\begin{aligned} \frac{\partial I}{\partial \varepsilon} = \int_{-\infty}^{\infty} \Bigg[& 2 \cdot \left| \frac{N(f)}{\{C_t(f) + \varepsilon\delta(f)\}\, W_{\text{total}}(f)} \right| \cdot \frac{1}{2 \left| \frac{N(f)}{\{C_t(f) + \varepsilon\delta(f)\} W_{\text{total}}(f)} \right|} \\ & \cdot \left\{ \frac{\partial}{\partial \varepsilon} \left(\frac{N^*(f)}{\{C_t^*(f) + \varepsilon^*\delta^*(f)\}\, W_{\text{total}}^*(f)} \right) \cdot \frac{N(f)}{\{C_t(f) + \varepsilon\delta(f)\}\, W_{\text{total}}(f)} + \frac{N^*(f)}{\{C_t^*(f) + \varepsilon^*\delta^*(f)\}\, W_{\text{total}}^*(f)} \right. \\ & \left. \cdot \frac{\partial}{\partial \varepsilon} \left(\frac{N(f)}{\{C_t(f) + \varepsilon\delta(f)\}\, W_{\text{total}}(f)} \right) + \mu\delta(f) \right\} \Bigg] df \end{aligned} \tag{A-4}$$

Here, the first term of the right side is zero. Thus,

$$\begin{aligned} \frac{\partial I}{\partial \varepsilon} &= \int_{-\infty}^{\infty} \left\{ \frac{N^*(f)}{\{C_t^*(f) + \varepsilon^*\delta^*(f)\}\, W_{\text{total}}^*(f)} \cdot \frac{-N(f)\,\delta(f)\, W_{\text{total}}(f)}{\left[\{C_t(f) + \varepsilon\delta(f)\}\, W_{\text{total}}(f)\right]^2} + \mu\delta(f) \right\} df \\ &= \int_{-\infty}^{\infty} \left\{ \frac{-|N(f)|^2}{|\{C_t(f) + \varepsilon\delta(f)\}\, W_{\text{total}}(f)|^2} \cdot \frac{1}{C_t(f) + \varepsilon\delta(f)} + \mu \right\} \delta(f)\, df \end{aligned} \tag{A-5}$$

When ε tends to zero,

$$\left.\frac{\partial I}{\partial \varepsilon}\right|_{\varepsilon=0} = \int_{-\infty}^{\infty} \left\{ \frac{-\left|N\left(f\right)\right|^2}{\left|C_t\left(f\right) W_{\text{total}}\left(f\right)\right|^2} \cdot \frac{1}{C_t\left(f\right)} + \mu \right\} \delta\left(f\right) df \tag{A-6}$$

If $\frac{\partial I}{\partial \varepsilon}|_{\varepsilon=0} = 0$ regardless of ε,

$$\frac{-\left|N\left(f\right)\right|^2}{\left|C_t\left(f\right) W_{\text{total}}\left(f\right)\right|^2} \cdot \frac{1}{C_t\left(f\right)} + \mu = 0 \tag{A-7}$$

$$\mu C_t\left(f\right)\left|C_t\left(f\right)\right|^2 = \left|\frac{N\left(f\right)}{W_{\text{total}}\left(f\right)}\right|^2 \tag{A-8}$$

Thus $C_t(f)$ is given by

$$C_t\left(f\right) = \mu_t \left|\frac{N\left(f\right)}{W_{\text{total}}\left(f\right)}\right|^{\frac{2}{3}} \tag{A-9}$$

Note that the phase response of the pre-emphasis filter is not a concern because adaptive post-compensation filters in the digital coherent receiver automatically adjust the phase.

References

[1] G. Bosco, V. Curri, A. Carena, P. Poggiolini, and F. Forghieri, "On the performance of Nyquist-WDM terabit superchannels based on PM-BPSK, PM-QPSK, PM-8QAM or PM-16QAM subcarriers," *IEEE/OSA J. Lightw. Technol.*, vol. 29, no. 1, pp. 53–61, Jan. 2011.

[2] T. Sasai, M. Nakamura, E. Yamazaki, S. Yamamoto, H. Nishizawa, and Y. Kisaka, "Digital backpropagation for optical path monitoring: Loss profile and passband narrowing estimation," in *Proc. 2020 Eur. Conf. Opt. Commun.*, Dec. 2020, Paper Tu2D-1.

[3] I. F. de J. Ruiz, A. Ghazisaeidi, T. Zami, S. Louis, and B. Lavigne, "An accurate model for system performance analysis of optical fibre networks with in-line filtering," in *Proc. 2019 Eur. Conf. Opt. Commun.*, Sep. 2019, Paper P78.

[4] K. Okamura, S. Yamaoka, Y. Mori, H. Hasegawa, and K. Sato, "Evaluation of WSS characteristics in highly dense WDM networks," in *Proc. 2019 Optoelectron. Commun. Conf. /Int. Conf. Photon. Switching Comput.*, 2019, Paper MF2-5.

[5] R. Shiraki, Y. Mori, H. Hasegawa, and K. Sato, "Design and evaluation of quasi-Nyquist WDM networks utilizing widely deployed wavelength-selective switches," *Opt. Exp.*, vol. 27, no. 13, pp. 18549–18560, 2019.

[6] T. Zami, I. F. de J. Ruiz, A. Ghazisaeidi, and B. Lavigne, "Growing impact of optical filtering in future WDM networks," in *Proc. 2019 Opt. Fiber Commun. Conf.*, 2019, Paper M1A.6.

[7] J. Pan and S. Tibuleac, "Filtering and crosstalk penalties for PDM-8QAM/16QAM super-channels in DWDM networks using broadcast-and-select and route-and-select ROADMs," in *Proc. 2016 Opt. Fiber Commun. Conf.*, 2016, Paper W2A.49.

[8] A. Morea, J. Renaudier, T. Zami, A. Ghazisaeidi, and O. Bertran-Pardo, "Throughput comparison between 50-GHz and 37.5-GHz grid transparent networks," *IEEE/OSA J. Opt. Commun. Netw.*, vol. 7, no. 2, pp. A293–A300, Feb. 2015.

[9] M. Filer and S. Tibuleac, "Cascaded ROADM tolerance of mQAM optical signals employing nyquist shaping," in *Proc. 2014 IEEE Photon. Conf.*, 2014, Paper TuF1.2.

[10] M. Filer and S. Tibuleac, "N-degree ROADM architecture comparison: Broadcast-and select versus route-and-select in 120 Gb/s DP-QPSK transmission systems," in *Proc. 2014 Opt. Fiber Commun. Conf.*, 2014, Paper Th1I.2.

[11] A. Morea, J. Renaudier, A. Ghazisaeidi, O. Bertran-Pardo, and T. Zami, "Impact of reducing channel spacing from 50GHz to 37.5GHz in fully transparent meshed networks," in *Proc. 2014 Opt. Fiber Commun. Conf.*, 2014, Paper Th1E.4.

[12] M. S. Frauk and S. J. Savory, "Digital signal processing for coherent transceivers employing multilevel formats," *IEEE/OSA J. Lightw. Technol.*, vol. 35, no. 5, pp. 1125–1141, Mar. 2017.

[13] K. Kikuchi, "Fundamentals of coherent optical fiber communications," *IEEE/OSA J. Lightw. Technol.*, vol. 34, no. 1, pp. 157–179, Jan. 2016.

[14] S. Yamaoka, Y. Mori, H. Hasegawa, and K. Sato, "Novel demodulation framework based on quadrature duobinary/quaternary/octernary spectrum shaping and MLSE for mitigating spectrum narrowing caused by node traversals," in *Proc. 2018 Eur. Conf. Opt. Commun.*, 2018, Paper Mo4F.5.

[15] Y. Mori, H. Hasegawa, and K. Sato, "Joint pre-, inline-, and post-compensation of spectrum narrowing caused by traversing multiple optical nodes," in *Proc. 2017 Eur. Conf. Opt. Commun.*, 2017, Paper P1.SC3.45.

[16] J. Pan and S. Tibuleac, "Real-time ROADM filtering penalty characterization and generalized precompensation for flexible grid networks," *IEEE Photon. J.*, vol. 9, no. 3, Jun. 2017, Art. no. 7202210.

[17] J. Zhang, J. Yu, N. Chi, and H. C. Chen, "Time-domain digital pre-equalization for band-limited signals based on receiver-side adaptive equalizers," *Opt. Exp.*, vol. 22, no. 17, pp. 20515–20529, 2014.

[18] J. Proakis and M. Salehi, *Digital Communications*. New York, NY, USA: McGraw-Hill, 2008.

[19] Q. Hu, F. Buchali, M. Chagnon, K. Schuh, and H. Bülow, "3.6-Tbps Duobinary 16-QAM transmission with improved tolerance to cascaded ROADM filtering penalty," in *Proc. 2018 Eur. Conf. Opt. Commun.*, 2018, Paper Tu3G.1.
[20] J. Yu *et al.*, "Transmission of 8 × 480-Gb/s super-Nyquist-filtering 9-QAM-like signal at 100 GHz-grid over 5000-km SMF-28 and twenty-five 100 GHz-grid ROADMs," *Opt. Exp.*, vol. 21, no. 13, pp. 15686–15691, 2013.
[21] J. H. Chang, K. Y. Cho, H. Y. Choi, Y. Takushima, and Y. C. Chung, "Filtering tolerance of 108-Gb/s polmux quadrature duobinary signal on 25-GHz grid," in *Proc. 2011 Opt. Fiber Commun. Conf.*, 2011, Paper OMR4.
[22] K. Okamura, Y. Mori, and H. Hasegawa, "Joint pre-emphasis and partial-response coding for spectrum narrowing caused by repeated optical-node traversal in ultra-dense WDM networks," in *Proc. 2020 Eur. Conf. Opt. Commun.*, 2020, Paper Mo2D-8.
[23] T. Rahman *et al.*, "On the mitigation of optical filtering penalties originating from ROADM cascade," *IEEE Photon. Technol. Lett.*, vol. 26, no. 2, pp. 154–157, Jan. 2014.
[24] S. L. Woodward, M. D. Feuler, and P. Palacharla, "ROADM-Node architectures for reconfigurable photonic networks," in *Optical Fiber Telecommunications VIB*, I. Kaminow, T. Li, and A. Willner, Eds., Cambridge, MA, USA: Academic Press, 2013.
[25] C. Pulikkaseril, L. A. Stewart, M. A. F. Roelens, G. W. Baxter, S. Poole, and S. Frisken, "Spectral modeling of channel band shapes in wavelength selective switches," *Opt. Exp.*, vol. 19, no. 9, pp. 8458–8470, 2011.
[26] G. P. Agrawal, *Nonlinear Fiber Optics*. Cambridge, MA, USA: Academic Press, 2012.
[27] D. Chang *et al.*, "LDPC convolutional codes using layered decoding algorithm for high speed coherent optical transmission," in *Proc. 2012 Opt. Fiber Commun. Conf. (OFC)*, 2012, Paper OW1H.4.
[28] G. Forney, "Maximum-likelihood sequence estimation of digital sequences in the presence of intersymbol interference," *IEEE Trans. Inf. Theory*, vol. IT-18, no. 3, pp. 363–378, May 1972.